



## Effect of solution heat treatment on the stress-induced martensite transformation in two new titanium alloys



C. Li<sup>a</sup>, J. Chen<sup>a,\*</sup>, Y.J. Ren<sup>a,\*</sup>, W. Li<sup>a</sup>, J.J. He<sup>a</sup>, J.H. Chen<sup>b</sup>

<sup>a</sup>Key Laboratory of Efficient and Clean Energy Utilization, College of Hunan Province, School of Energy and Power Engineering, Changsha University of Science and Technology, Changsha, Hunan 410114, China

<sup>b</sup>College of Materials Science and Engineering, Hunan University, Changsha, Hunan 410082, China

### ARTICLE INFO

#### Article history:

Received 16 March 2015

Received in revised form 10 April 2015

Accepted 11 April 2015

Available online 16 April 2015

#### Keywords:

Solution treatment

Stress-induced martensite transformation

Microstructure

Ti alloys

### ABSTRACT

Ti–10V–2Cr–3Al and Ti–10V–1Fe–3Al alloys are newly designed two phase titanium alloy for stress-induced martensite (SIM) transformation on the basis of Ti–10V–2Fe–3Al alloy. The effect of solution heat treatment on the SIM transformation in these two alloys was studied through microstructural observation and mechanical property test. The results show that, after  $\beta$ ,  $\alpha + \beta$  and  $\beta + (\alpha + \beta)$  solution treatments, most of the samples contain a highly metastable  $\beta$  microstructure. Under compression loading, the  $\beta$  phase transform to a martensite. The stress at which  $\beta$  to  $\alpha'$  transformation is triggered is very stable to the solution time. The pre-existing thermal martensite has an obstructive effect on SIM transformation. In  $\beta + (\alpha + \beta)$  solution conditions, tuning the volume fraction of the  $\alpha$  phase leads to a sufficiently stable  $\beta$  phase so that no martensite is formed under deformation and only slip is activated. Moreover, the effect of solution temperature on triggering stress is more intense compared with that of solution time.

© 2015 Elsevier B.V. All rights reserved.

## 1. Introduction

Titanium and its alloys have become an object of wide research due to their desirable properties like high specific strength, considerable ductility, excellent corrosion resistance and good biocompatibility. These properties have made titanium alloys promising materials for metallic structures in the aircraft and marine industries, for operation under the conditions of chemical atmosphere and for biological applications [1]. Phase transformation resulting from the deformation of metals, like steel, are intentionally used to improve properties [2,3]. It is generally accepted that metastable grades of  $\beta$  titanium alloys may undergo deformation via the formation of stress-induced martensite (SIM) [4–15]. Control of this mechanism could provide a new route to the optimization of the load bearing capabilities of titanium alloys. Earlier transformation plasticity studies in titanium alloys like Ti–10V–2Fe–3Al [16],  $\beta$ -Cez [17], and Ti–8.0Mo–3.9Nb–2.0V–3.1Al [18] have shown that the stress-induced martensite formation starting from a metastable  $\beta$  phase, can indeed result in an improved balance of strength and ductility. Therefore, a better understanding of the critical stress levels for the stress-induced martensite formation is

important for the optimization of the mechanical properties of titanium alloys and in particular their load bearing capabilities.

Ti–10V–2Fe–3Al alloy is a deep hardenable near beta titanium alloy. It was developed by TIMET company over 40 years ago to provide weight savings in forged aircraft undercarriage component, such as landing gear system of airplanes in Boeing 777 and Airbus 380 [19]. In the present study, two novel titanium alloys which offer proper heat treatments can show stress-induced martensitic transformation (Ti–10V–2Cr–3Al and Ti–10V–1Fe–3Al) have been prepared on the basis of the concepts and results of earlier work on the Ti–10V–2Fe–3Al alloy [20,21]. However, as two alloys are newly developed, information within the literature critical to its further development and application is very limited. The relationship between microstructure and the mechanical properties of these two alloys has not been fully understood. Besides its chemical composition, however, the mechanical property of Ti alloys also depends critically upon the prior solution condition, especially whether the alloy undergoes a solution treatment at above or below the  $\beta$  transus temperature. These factors control the very earliest stages of  $\beta$  decomposition and the subsequent phase transformation that determine the actual hardening response. Therefore, for the current investigation, attention was focused mainly on elucidating the influence of solution treatment on the stress induced martensite transformation.

\* Corresponding authors.

E-mail addresses: [csuost@126.com](mailto:csuost@126.com) (J. Chen), [ryj1008@163.com](mailto:ryj1008@163.com) (Y.J. Ren).

## 2. Materials and experiments

### 2.1. Defining new alloys

Inspired by the Ti–10V–2Fe–3Al alloy displaying a tunable SIM behavior, new alloy compositions having the potential to optimally exhibit such effect have been designed as follows. The main criteria considered for designing new alloy compositions with a (quantified) stability of in the 100%  $\beta$  state are the molybdenum equivalency and the martensite start temperature  $M_s$ . Both depend on the chemical composition according to Eqs. (1) and (2) respectively [1,12]

$$Mo_{eq} = 1.00Mo_{wt\%} + 0.28Nb_{wt\%} + 0.22Ta_{wt\%} + 0.67V_{wt\%} + 1.6Cr_{wt\%} + 2.9Fe_{wt\%} - 1.00Al_{wt\%} \quad (1)$$

$$M_s \text{ (K)} = 1156 - 150Fe_{wt\%} - 96Cr_{wt\%} - 49Mo_{wt\%} - 37V_{wt\%} - 17Nb_{wt\%} - 7Zr_{wt\%} + 15Al_{wt\%} \quad (2)$$

Fig. 1 shows the phase stability map calculated for titanium alloys. The reference alloy Ti–10V–2Fe–3Al is situated in the upper left direction relative to the two new alloys, with a relatively a higher  $Mo_{eq}$  value and lower  $M_s$  temperature. This stability value is assumed to apply to both a fully  $\beta$  microstructure and to the  $\beta$  fraction in a mixed  $\alpha$ – $\beta$  microstructure. As the formation of the  $\alpha$  fraction during annealing in the intercritical region induces compositional changes due to alloying element partitioning, the stability of the  $\beta$  fraction increases with the  $\alpha$  fraction formed. For the reference Ti–10V–2Fe–3Al alloy, SIM behavior was observed for its  $\beta$  fraction under the conditions  $\sim 9 < Mo_{eq} \beta \text{ fraction} < \sim 16$  or  $\sim 550 \text{ K} < M_s < \sim 200 \text{ K}$ . The lower boundary  $Mo_{eq}$  value of  $\sim 9$  (corresponding to the upper boundary for the  $M_s$  temperature) is determined by the chemical composition of the base alloy while the upper  $Mo_{eq}$  boundary value of  $\sim 16$  was determined from the result of an increased (chemical) stability of the  $\beta$  phase. In order to get a more accurate and generally defined compositional or compositional/microstructural window for controlled SIM formation, two novel titanium alloys have been designed and prepared with a nominal composition Ti–10V–2Cr–3Al and Ti–10V–1Fe–3Al. Their stability values for the fully  $\beta$  state are also indicated in Fig. 1.

The new alloys Ti–10V–2Cr–3Al and Ti–10V–1Fe–3Al have been fabricated on a laboratory scale by the Institute of Metal Research, Chinese Academy of Sciences, Shenyang, China. Each alloy weighing about 5 kg was obtained in a forged condition. The chemical compositions of the as-received alloys, measured by the wet analysis method, are listed in Table 1. The  $\beta$  transus temperatures for the materials in its as-received state have been measured using dilatometer. The measured  $\beta$  transus values of Ti–10V–2Cr–3Al alloy and Ti–10V–1Fe–3Al alloy are approximately  $810 \pm 5 \text{ }^\circ\text{C}$  and  $830 \pm 5 \text{ }^\circ\text{C}$ , respectively. The as-received microstructure of the Ti–10V–2Cr–3Al alloy shows a high volume fraction of very fine  $\alpha$  phase (Fig. 2(a)). The Ti–10V–1Fe–3Al alloy shows a lower volume fraction of the  $\alpha$  phase which has a mixed morphology (Fig. 2(b)).

### 2.2. Experimental methods

From the as-received thick slab, cylindrical samples of 4 mm diameter and 7 mm length were machined using electrical discharge machining (EDM). The very thin oxidized outer surface layer was removed by careful mechanical polishing prior to further experimentation. The cylindrical samples were solution treated at various temperatures using a quartz tube filled with argon gas, and water quenched to room temperature. For microstructure analysis additional electropolishing with a solution of 36 ml perchloric acid, 390 ml methanol, 350 ml ethylene glycol and

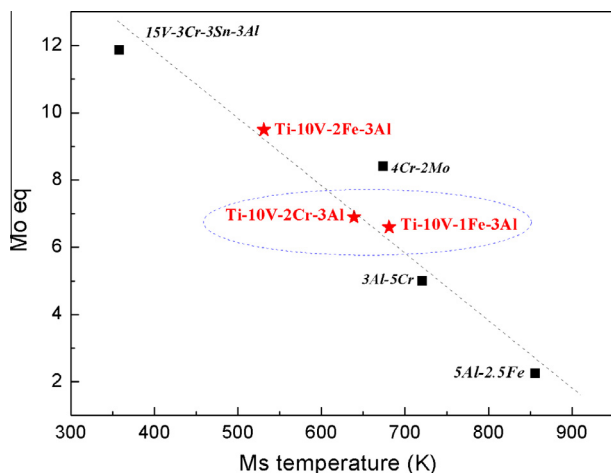


Fig. 1. Validation of the designed new alloys composition in the  $Mo_{eq}$  vs  $M_s$  map.

Table 1

The chemical compositions of the fabricated new alloys (in wt.%).

	V	Al	Cr	Fe	O	C	N	Ti
Ti–10V–2Cr–3Al	10.6	3.1	2.18	–	0.1	0.05	0.013	Bal.
Ti–10V–1Fe–3Al	9.97	3.02	–	0.97	0.11	0.051	0.014	Bal.

24 ml water was used in order to avoid any transformation of metastable  $\beta$  phase to martensite during mechanical polishing. Standard Kroll's reagent (3 ml HF + 6 ml  $\text{HNO}_3$  + 100 ml  $\text{H}_2\text{O}$ ) was used for revealing the various phases in Ti–10V–1Fe–3Al alloy, but a modified etchant solution for Ti–10V–2Cr–3Al alloy was employed to reveal the microstructure properly (5 ml HF + 10 ml  $\text{HNO}_3$  + 30 ml  $\text{H}_2\text{O}$ ). The microstructures were determined using a field emission scanning electron microscope (FE-SEM) and an optical microscope. Detailed microstructural investigation was carried out by transmission electron microscopy (TEM). The thin foils required for the TEM observations were prepared by a standard polishing procedure and a twin-jet electro-polishing technique using a solution of 21 vol% perchloric acid, 50 vol% methanol and 29 vol% n-butyl alcohol at  $-25 \text{ }^\circ\text{C}$ . The mechanical properties for the various heat treatments were assessed by compression testing at room temperature at a strain rate of  $10^{-3} \text{ s}^{-1}$  in a Gleeble 1500 thermo-mechanical machine. For each condition, 3 samples were deformed. In order to avoid friction between the anvils and the sample surface, a lubricant (Lubriplate<sup>®</sup>) was used.

## 3. Results and discussions

Different solution heating schedules have been imposed to create different microstructures. For organizational purposes, the results of the study of these two alloys can be sub-divided into three sub-sections according to their microstructural comparability. These are listed below:

- (1)  $\beta$  solution treatment conditions
- (2)  $(\alpha + \beta)$  solution treatment conditions
- (3)  $\beta + (\alpha + \beta)$  solution treatment conditions

Each of these topics will be separately discussed. The effect of these various microstructural modifications on the SIM transformation in the two alloys will also be identified.

### 3.1. $\beta$ solution treatment conditions

To determine the influence of the solution time in the  $\beta$  phase field, samples were directly solution treated above the  $\beta$ -transus. The following heat treatments were used:  $900 \text{ }^\circ\text{C}/5 \text{ min}$ ,  $900 \text{ }^\circ\text{C}/15 \text{ min}$ ,  $900 \text{ }^\circ\text{C}/25 \text{ min}$ . Fig. 3(a) shows the optical micrograph of water quenched Ti–10V–2Cr–3Al alloy subjected to  $\beta$  solution treated condition. The microstructure consists of an equiaxed  $\beta$  grain structure and fine needle-like martensite which was confirmed to be hexagonal  $\alpha'$  martensite [22]. For Ti–10V–1Fe–3Al, the alloy after  $\beta$  solution treatment also exhibited a  $\beta$  phase structure and hexagonal  $\alpha'$  martensite which is composed of long orthogonally oriented plates and has an acicular morphology, as showed in Fig. 3(b). On the other hand, longer solution time facilitates the growth of equiaxed  $\beta$  grains. The grain size increases as the solution time is extended ( $150\text{--}180 \text{ }\mu\text{m}$  for 5 min and  $200\text{--}220 \text{ }\mu\text{m}$  for 25 min).

The mechanical properties of heat treated samples were evaluated by compression test. Typical stress–strain curves for the alloys after different heat treatment are shown in Fig. 4. It can be seen that the nature of stress–strain curves is similar for all heating conditions. These figures show that two alloys exhibit a double yield phenomenon and hence stress-induced martensitic transformations at all heating conditions. The lower and upper yield stress values of the linear (non-elastic) section of the strain–stress curves, being the start and the end of the SIM transformation, have been determined by the method of tangents intersection, as marked by arrows in Fig. 4(a). At the beginning of the transformation,

Download English Version:

<https://daneshyari.com/en/article/7998881>

Download Persian Version:

<https://daneshyari.com/article/7998881>

[Daneshyari.com](https://daneshyari.com)